

Mean field studies of high-spin properties in the $A \sim 30$ and 60 regions of superdeformation.

A. V. Afanasjev¹, P. Ring,

Physik-Department der Technischen Universität München, D-85747 Garching, Germany

I. Ragnarsson

Department of Mathematical Physics, Lund Institute of Technology, S-22100, Lund, Sweden

Abstract:

The importance of deformation changes and the possible role of proton-neutron pairing correlations on the properties of paired band crossings at superdeformation in the $A \sim 60$ mass region have been analyzed. The present analysis, supported in part by the cranked relativistic Hartree-Bogoliubov calculations for the SD band in ^{60}Zn , suggests that when going from ^{60}Zn to neighboring odd nuclei the properties of paired band crossings are strongly influenced by deformation changes. A number of questions related to the superdeformation in the $A \sim 30$ mass region has been studied with the cranked relativistic mean field theory and the configuration-dependent cranked Nilsson-Strutinsky approach.

1 Introduction

Superdeformation at high spin is by now a wide-spread phenomenon across the periodic table. In recent years, the attention of the high-spin community has been shifted to the lighter nuclei in the vicinity of the $N \approx Z$ line after the discovery of superdeformed (SD) bands in ^{62}Zn [1] and neighboring nuclei and in ^{36}Ar [2]. These regions of superdeformation are characterized by several distinct features which are either not present or much less visible at superdeformation in heavier nuclei. First, the relative polarization effects from the individual intruder and extruder orbitals are expected to be much stronger than in heavier mass regions. Second, the limited angular momentum content of specific configurations is expected to play a significant role in the definition of the rotational properties of the SD bands [3]. For example, a considerable decrease of the dynamic moment of inertia ($J^{(2)}$) with respect to the kinematic moment of inertia ($J^{(1)}$) has been observed in the SD bands of the $A \sim 60$ mass region at the highest rotational frequencies. This feature is similar to the one seen in smoothly terminating bands in the $A \sim 110$ and $A \sim 60$ regions [4]. In the $A \sim 30$ mass region, the recently discovered SD band in ^{36}Ar has been observed up to terminating state at $I^\pi = 16^+$ [2]. The third distinct feature is related to the possible effects emerging from the proton-neutron pairing correlations [5, 6].

In the present manuscript a number of issues related to the superdeformation in these mass regions is studied mainly in the framework of the cranked versions of the relativistic mean field theory

¹on leave of absence from the Laboratory of Radiation Physics, Institute of Solid State Physics, University of Latvia, LV 2169 Salaspils, Miera str. 31, Latvia

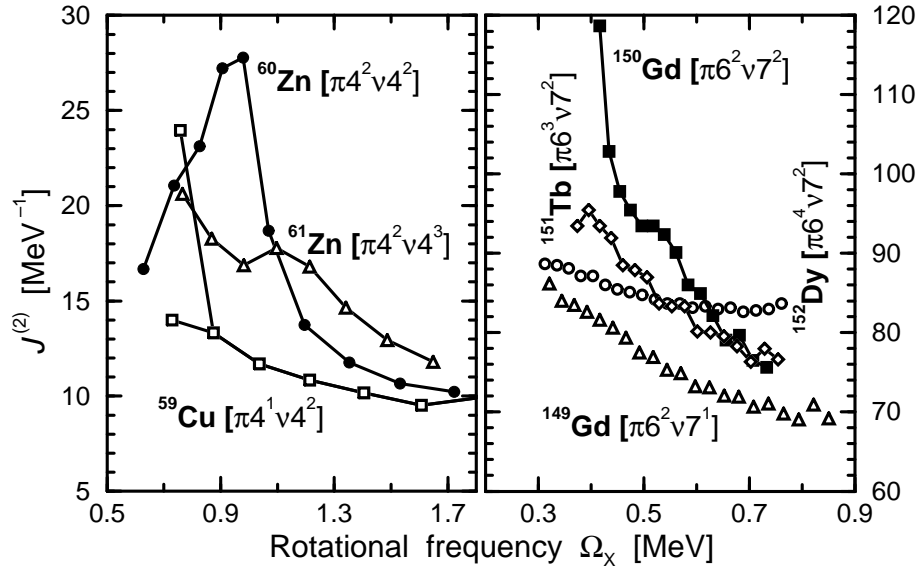


Figure 1: Dynamic moments of inertia of the yrast SD bands in the $A \sim 60$ (left panel) and $A \sim 150$ (right panel) mass regions. The configurations are labeled by the number of occupied high- N intruder orbitals. For details of the configuration assignment in the $A \sim 150$ mass region see Refs. [8, 14] and references therein.

[7, 8, 9]. In addition, the general structure of the yrast lines in the $A \sim 30$ mass region emerging from the coexistence of collective and non-collective structures has been analyzed within the configuration-dependent cranked Nilsson-Strutinsky approach [4].

2 The $A \sim 60$ $N \approx Z$ mass region.

It is well known that the high-spin properties of the nuclei in the $A \sim 60$ region are dominated by a variety of phenomena among which smooth band termination [10, 11] and superdeformation (SD) [1, 12, 13] are reliably established today. The cranked relativistic mean field (CRMf) theory, in which the pairing correlations are neglected, has been very successfully applied to the description of the properties of a number of SD bands in this mass region, see Refs. [3, 6, 12, 13] for details. In the present contribution, we will concentrate on the properties of SD bands in the $^{60,61}\text{Zn}$ and ^{59}Cu nuclei which have been in the focus of the recent discussions [5, 6].

The experimental dynamic moments of inertia $J^{(2)}$ of these bands are shown in Fig. 1. One can see that the SD band in the $N = Z$ ^{60}Zn nucleus shows a large jump in $J^{(2)}$ at rotational frequency $\Omega_x \sim 1.0$ MeV. It was suggested in Ref. [12] that simultaneous alignments of the first pairs of the $g_{9/2}$ protons and $g_{9/2}$ neutrons are responsible for this observed feature. Such an interpretation was based on the fact that in the calculations without pairing the assigned configuration has 2 $g_{9/2}$ protons and 2 $g_{9/2}$ neutrons. On the contrary, the SD band in the $N = Z + 1$ ^{61}Zn nucleus shows only a small bump at $\Omega_x \sim 1.15$ MeV indicating a nearly complete blocking of the alignment observed in ^{60}Zn . Because of this feature, the authors of Ref. [5] questioned the interpretation of the SD band in ^{60}Zn given above. Indeed, assuming the same deformation of the SD bands in these two nuclei and that the jump in $J^{(2)}$ for the SD band in ^{60}Zn originates from the simultaneous alignments of independent $g_{9/2}$ proton and neutron pairs, it is reasonable to expect that the odd neutron in ^{61}Zn should only block the neutron contribution to the alignment, while the proton contribution should result in an alignment roughly half of that observed in ^{60}Zn .

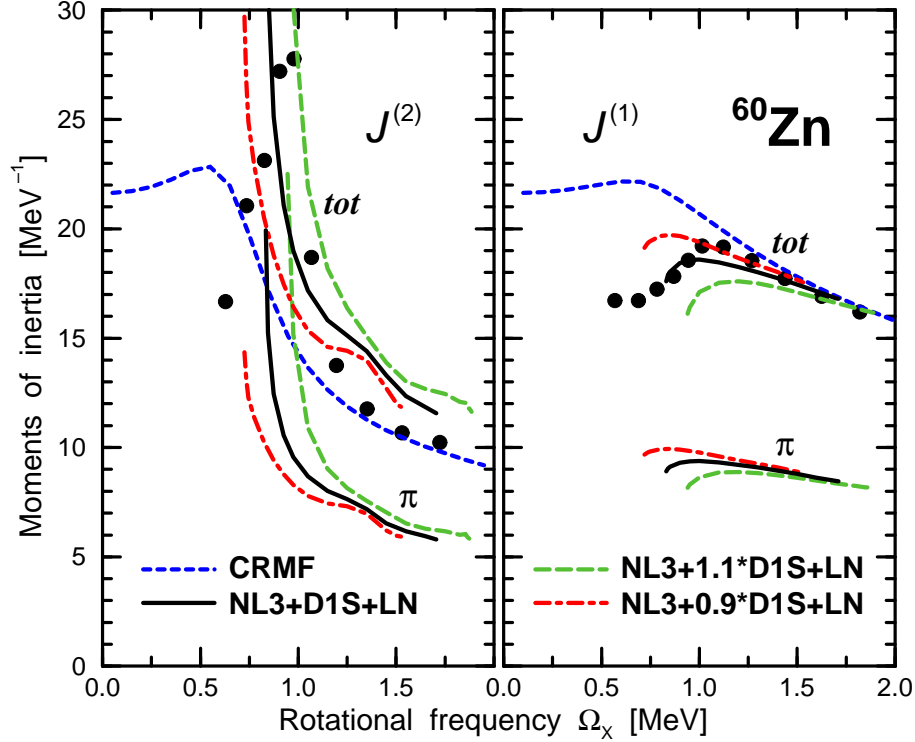


Figure 2: Experimental (solid circles) and calculated (lines) kinematic and dynamic moments of inertia of the SD band in ^{60}Zn . The notation of the lines is given in the figure. Note that the CRHB results are shown only in the frequency range where convergence to the self-consistent SD solution is obtained. At low rotational frequencies, the solution converges to the normal-deformed minimum instead of the SD one, most likely due to the small barrier between these two minima. This, in principle, can be overcome by an additional constraint on the quadrupole moment. At high frequencies, no convergence has been obtained after 200 iterations due to very weak pairing correlations, see Fig. 3. Since the proton and neutron contributions to the total dynamic and kinematic moments of inertia are almost identical, only the proton contributions are shown on the bottom of the panels.

Thus it was suggested that the observed features may be due to $T = 0$ proton-neutron pairing correlations present in ^{60}Zn , namely the peak in the $J^{(2)}$ of ^{60}Zn is due to the crossing of the $T = 1$ and $T = 0$ bands. On the other hand, the analysis performed in Refs. [15, 16] within the single- j subshell model and the cranked shell model at fixed deformation indicates that the frequency of the first band crossing in the $N = Z$ nuclei is sensitive to the $T = 1$ component of the two-body proton-neutron interaction but not to the $T = 0$ component. The first alignment appears to be delayed by the $T = 1$ proton-neutron pairing field when the intruder shell becomes more symmetrically filled. Similar to ^{61}Zn , a SD high-spin band has been observed experimentally also in the $Z = N - 1$ ^{59}Cu nucleus, see Fig. 1. However, it is more complicated because of a branching at low spin in the observed SD band, which gives two $I = 25/2$ states, see Fig. 1 in Ref. [6]. Depending on which state is assumed to be the lowest observed state in the SD band, the $J^{(2)}$ moment of inertia is either smooth or has a very large jump at the lowest frequencies. In the latter case, it might be considered as a possible argument in favor of the delay of the first band crossing due to the $T = 1$ proton-neutron pairing field discussed above.

The considerations given above neglect the deformation changes between the SD bands which can play a considerable role in the definition of the properties of the first paired band crossings. It is interesting to note that features similar to the ones seen in the ^{59}Cu - ^{60}Zn - ^{61}Zn chain have been observed earlier in the $A \sim 150$ region of superdeformation, see Fig. 1 and Ref. [8] for

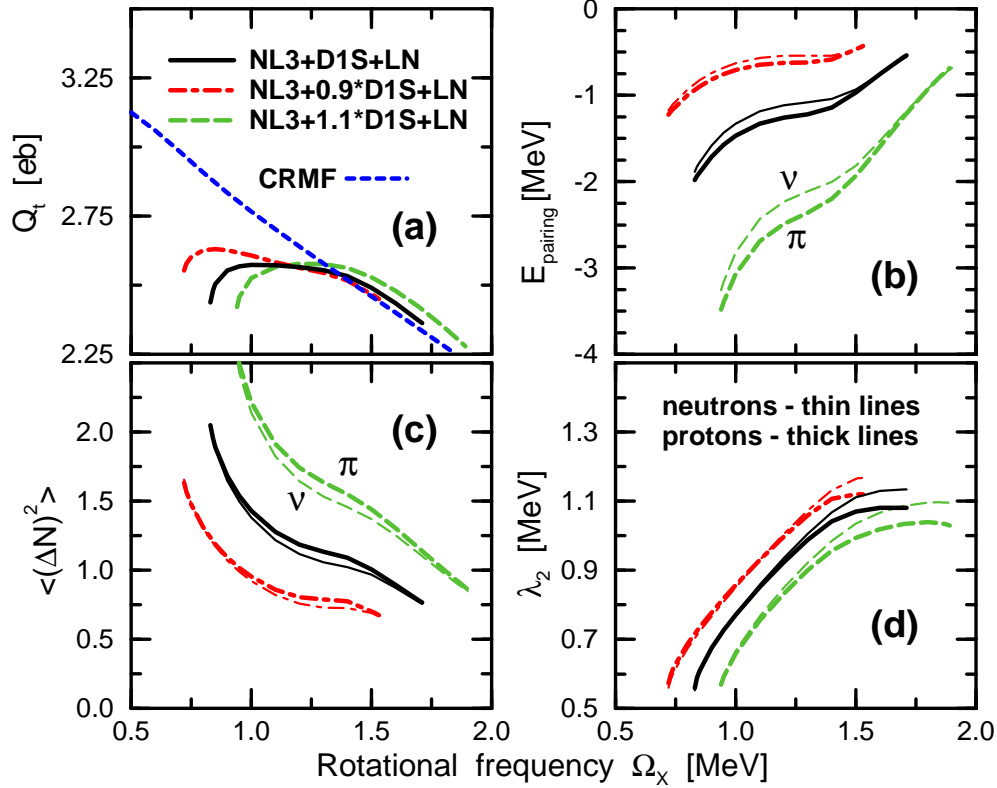


Figure 3: Calculated values of the transition quadrupole moments Q_t (panel (a)), pairing energies $E_{\text{pairing}} = -\frac{1}{2}\text{Tr}(\Delta\kappa)$ (panel (b)), particle number fluctuations $\langle(\Delta N)^2\rangle$ (panel (c)) and λ_2 (panel (d)) in ^{60}Zn as a function of rotational frequency Ω_x obtained for the solutions presented in Fig. 2. The notation of the lines is given in the figure.

details. The large jump and the subsequent small bump in $J^{(2)}$ of the yrast SD band in ^{150}Gd at $\Omega_x < 0.6$ MeV have been explained within the cranked Nilsson-Strutinsky approach based on a Woods-Saxon potential in terms of consecutive neutron and proton alignments [17]. The configuration of this band is $\pi 6^2\nu 7^2$. The addition of one $N = 6$ proton (band $^{151}\text{Tb}(1)$) blocks not only the proton paired band crossing (which is expected from simple blocking arguments) but also the neutron paired band crossing. Similarly the configuration of the yrast SD band in ^{152}Dy does not show any signs of the 'expected' proton and neutron paired band crossings. In the same fashion, there are no clear signs of proton paired band crossing in the dynamic moment of inertia of the $^{149}\text{Gd}(1)$ band. These examples show the strong dependence of the properties of the 'expected' proton and neutron paired band crossings on the deformation in a system where the proton-neutron pairing correlations play no role. It is also reasonable to expect a similar impact of deformation changes on the properties of SD bands in the $A \sim 60$ region. It is especially true considering that the changes in transition quadrupole moments Q_t induced by additional particle(s) are relatively modest in the $A \sim 150$ region ($Q_t(^{152}\text{Dy})/Q_t(^{150}\text{Gd}) \approx 1.13$, $Q_t(^{151}\text{Tb})/Q_t(^{150}\text{Gd}) \approx 1.06$, $Q_t(^{149}\text{Gd})/Q_t(^{150}\text{Gd}) \approx 0.95$; these ratios are based on the results of the CRMF calculations, see Ref. [8]) as compared with the $A \sim 60$ region, where, for example, the calculated ratio is $Q_t(^{59}\text{Cu})/Q_t(^{60}\text{Zn}) \approx 0.82$ [6].

In order to shed some light on the properties of the SD band in ^{60}Zn , they have been studied within the cranked relativistic Hartree-Bogoliubov (CRHB) theory [9], which has been very successful in the description of SD bands in the $A \sim 190$ mass region [9, 18]. The calculations have been performed with the NL3 force for the RMF Lagrangian and D1S set for the Gogny force in the

particle-particle channel. Note that only like-particle pairing has been taken into account. In addition, approximate particle number projection has been performed by means of the Lipkin-Nogami method (further APNP(LN)). In the calculations all fermionic and bosonic states belonging to the shells up to $N_F = 12$ and $N_B = 16$ are taken into account and the basis deformation $\beta_0 = 0.4, \gamma = 0^\circ$ is used. The results of the calculations are shown in Figs. 2 and 3.

It is clearly seen in Fig. 2 that the rise in $J^{(2)}$ in ^{60}Zn with decreasing rotational frequency and the evolution of kinematic moment of inertia $J^{(2)}$ are reasonably well reproduced in the CRHB calculations with no additional parameters (lines indicated by NL3+D1S+LN). At rotational frequencies above the band crossing, the CRHB calculations overestimate the experimental dynamic moment of inertia by $\sim 10\%$. At these frequencies, the CRMF calculations without pairing describe the $J^{(2)}$ and $J^{(1)}$ moments almost perfectly. According to the CRHB calculations, the jump in $J^{(2)}$ originates from the simultaneous alignment of the first pairs of the $g_{9/2}$ protons and neutrons. This is contrary to the results obtained in the projected shell model [19] where the jump in $J^{(2)}$ originates from two successive band crossings.

Fig. 3 shows the results of the calculations for other quantities of interest. The pairing correlations in the ^{60}Zn SD band are much smaller than the ones calculated in the $A \sim 190$ mass region, compare Fig. 3b in the present manuscript with Fig. 4 in Ref. [9]. They decrease with increasing rotational frequency reflecting the Coriolis anti-pairing effect. Note also that the pairing collapse in the proton and neutron subsystems is observed in the calculations without APNP(LN). As a consequence of weak pairing correlations, the results of the calculations without pairing are very close to the ones with pairing at $\Omega_x \geq 1.25$ MeV for the physical observables of interest such as kinematic and dynamic moments of inertia (Fig. 2), and transition quadrupole moments (Fig. 3b). The CRHB calculations indicate a slight lowering of kinematic moments of inertia and transition quadrupole moments Q_t at the frequencies $\Omega_x < 1.25$ MeV as compared with the calculations without pairing.

The effect of the strength of the Gogny force on the results of the CRHB calculations has been investigated by introducing the scaling factor f into the Gogny force (see Ref. [9] for details). The results of the calculations with the scaling factors $f = 0.9$ (lines indicated by NL3+0.9*D1S+LN) and $f = 1.1$ (lines indicated by NL3+1.1*D1S+LN) are shown in Figs. 2 and 3. The effect of the scaling of the Gogny force is especially drastic on the pairing properties, see Fig. 3b,c. It has also considerable impact on the rotational properties at $\Omega_x < 1.25$ MeV, see Fig. 2. For example, the frequency of the paired band crossing is increased (decreased) by $\Delta\Omega_x \sim 0.135$ MeV when the strength of the Gogny force is increased (decreased) by 10%.

The essence of the present discussion of the properties of the SD bands in the ^{59}Cu - ^{60}Zn - ^{61}Zn nuclei is the question if the observed features are due to the effects of (i) deformation changes or (ii) $T = 1$ proton-neutron pairing interaction or (iii) combined effect of both of them. The similarity of the experimental situation in the nuclei around ^{60}Zn with the one around ^{150}Gd strongly suggests that the deformation changes should play an important role. The main features of paired band crossing in ^{60}Zn can be understood in the CRHB theory without an explicit proton-neutron pairing. However, this does by no means imply that there is no proton-neutron pairing field. Further development of the CRHB theory for description of the proton-neutron pairing is necessary in order to clarify how the balance between like-particle pairing and proton-neutron pairing is changed with increasing rotational frequency at superdeformation and how it affects the observed rotational properties.

One should also note that the approximate particle number projection by means of the Lipkin-Nogami method might be a poor approximation to the exact particle number projection in the regime of weak pairing correlations in rotating nuclei. For example, the particle number fluctuations $\langle(\Delta N)^2\rangle$ in the unprojected wave function are rather small in the ^{60}Zn SD band indicating that the breaking of gauge symmetry is small. Studies in the full configuration space with exact particle number projection are definitely needed in order to estimate the accuracy of the Lipkin-Nogami method in rotating nuclei in the weak pairing regime.

3 The $A \sim 32$ $N \approx Z$ mass region.

In the nuclei in the upper half of the sd -shell, high-spin bands are formed in configurations with particles excited to the fp -shell. Of special interest is the yrast SD configuration in ^{32}S which was predicted long ago, see e.g. Refs. [20, 21], but where the corresponding rotational band has not been observed at present. The question of superdeformation in this nucleus has been recently in the focus of a number of theoretical investigations within the microscopic theories based on the Skyrme [22, 23] and Gogny forces [24, 25]. Fig. 4 shows the calculated high-spin structure of this nucleus obtained in the CRMF theory with the NL3 parametrization [26] of the RMF Lagrangian. The lowest SD configuration in this nucleus is lowest in energy amongst collective structures in the spin range of $I = 10 - 22\hbar$ and contains two protons and two neutrons excited to the fp -shell (see Fig. 5). It has a $\pi 3^2\nu 3^2$ structure in terms of occupied intruder high- N orbitals. The calculated SD configuration is built from the magic 16 particle $\omega_\perp : \omega_z = 2 : 1$ configuration of the harmonic oscillator, which appears to be only slightly disturbed in realistic nuclear potentials.

The dynamic and kinematic moments of inertia of this configuration are shown in Fig. 4b. While at low rotational frequencies these moments are approximately equal, at high frequencies of $\Omega_x \sim 2.5$ MeV, the dynamic moment of inertia is approximately 60% of kinematic one. This feature is similar to the one which has been observed experimentally in the $A \sim 60$ mass region of superdeformation, see Refs. [3, 12] for details. It comes from the fact that it is not so much the deformation (at $I = 0$) of the configuration which determines if it is rigid-rotor-like ($J^{(1)} \approx J^{(2)}$) or not but rather how far away the configuration is from its “maximum” spin (see Refs. [3, 27] for more details). Indeed, the “maximum” spin of this configuration defined from the distribution of particles and holes at low spin is $I_{max} = 24\hbar$. The calculations also indicate a gradual drop of collectivity (i.e., a drop of transition quadrupole moment Q_t) with increasing spin, see Fig. 4. At higher rotational frequencies, the dynamic moments of inertia increases due to the admixture of the lowest $g_{9/2}$ orbitals indicating that the lowest SD configuration changes its character from $[2,2]$ to $[2(1),2(1)]$.

In many details the results of the CRMF calculations for the doubly-magic SD configuration in ^{32}S are similar to the ones obtained in the calculations based on the Skyrme and Gogny forces [22, 23, 24]. An interesting difference is essentially related to the signature splitting effects emerging from the time-odd components of the mean field. Some features of this effect will be discussed below, while full results of the investigation of superdeformation in the $A \sim 30$ mass region within the framework of the CRMF theory will be presented in a forthcoming article [28].

The signature separation induced by time-odd mean fields has been found earlier in the excited SD bands of ^{32}S in the cranked Hartree-Fock calculations based on the effective forces of the Skyrme type [22]. The clear advantage of the CRMF theory compared with this approach is the fact that

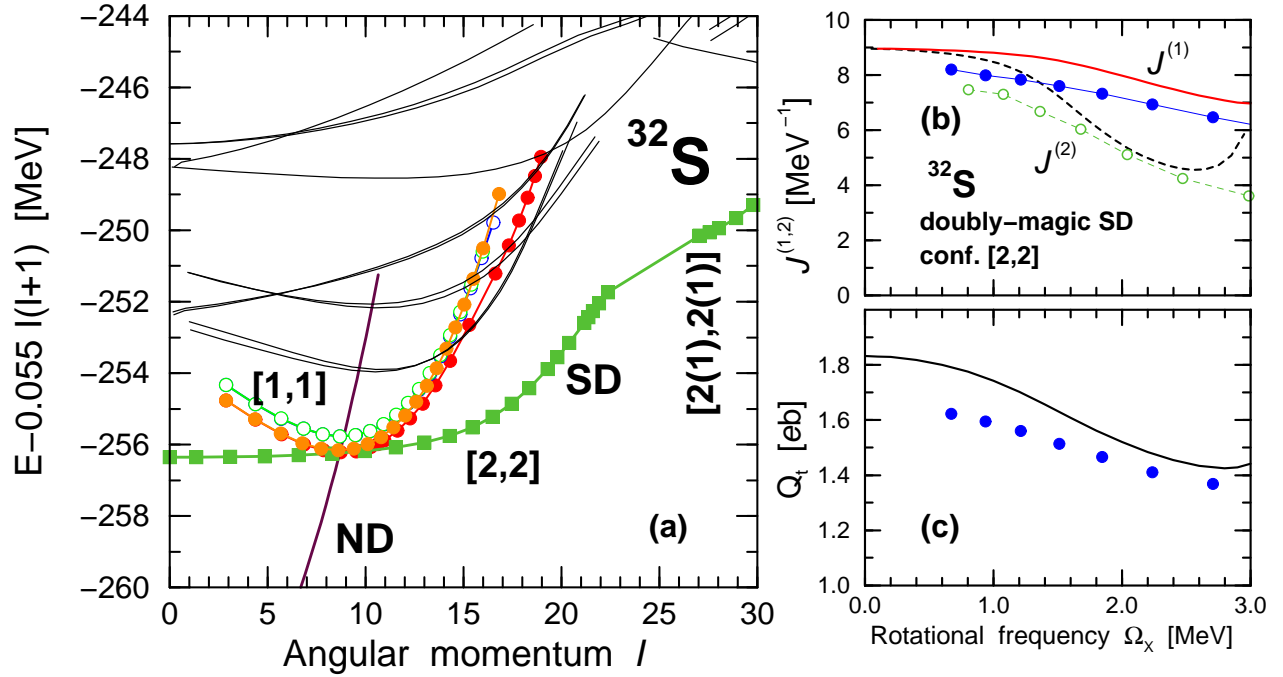


Figure 4: (a) The energies of SD configurations calculated in the CRMF theory with the rigid rotor reference subtracted. In addition, the lowest calculated collective states in the normal-deformed (ND) minimum are also shown. The configurations discussed in the manuscript are shown by the lines with symbols. Solid (open) symbols are used for total signature $r_{tot} = +1$ ($r_{tot} = -1$). Other excited SD configurations are shown by thin solid lines. The configurations are labeled by the shorthand labels $[p_1(p_2), n_1(n_2)]$, where p_1 (n_1) is the number of $f_{7/2}$ protons (neutrons) and p_2 (n_2) is the number of $g_{9/2}$ protons (neutrons). Note that p_2 (n_2) are omitted when the $g_{9/2}$ orbitals are not occupied. The kinematic ($J^{(1)}$) and dynamic ($J^{(2)}$) moments of inertia and transition quadrupole (Q_t) moments calculated for the doubly magic SD configuration $[2,2]$ in ^{32}S are shown in panels (b) and (c), respectively. For comparison, the CNS results for these quantities are shown by filled and open circles.

time-odd fields (emerging in this theory from nuclear magnetism) are defined in a unique way. In order to make a comparison between these two approaches straightforward, the CRMF calculations have been performed for the four excited SD configurations having the structure

$$\bullet \pi : h[330]1/2^- p[202]5/2^\pm \otimes \nu : h[330]1/2^- p[202]5/2^\pm (r_{tot} = \pm 1)$$

which display the signature separation induced by time-odd fields in Skyrme calculations. Here the configurations are labeled by the particles (p) and holes (h) with respect to the doubly-magic SD configuration in ^{32}S and superscripts to orbital labels are used to indicate the sign of the signature r for that orbital ($r = \pm i$). These configurations are shown by lines with circles in Fig. 4. When nuclear magnetism (time-odd mean fields) is neglected these four configurations are degenerate in energy at no rotation. This degeneracy is broken and additional binding, which depends on the total signature of the configuration (0.907 MeV for the $r_{tot} = +1$ configurations and 0.468 MeV for the $r_{tot} = -1$ configurations), is obtained when nuclear magnetism is taken into account. It is interesting to note that the NL1 and NLSH parametrizations of the RMF Lagrangian give very similar values of additional binding due to nuclear magnetism. The essential difference between relativistic and non-relativistic calculations lies in the size of the energy gap between the $r_{tot} = +1$ and $r_{tot} = -1$ configurations. This gap exceeds 2 MeV in Skyrme calculations, while it is significantly smaller in the CRMF calculations being around 0.45 MeV. In addition, the

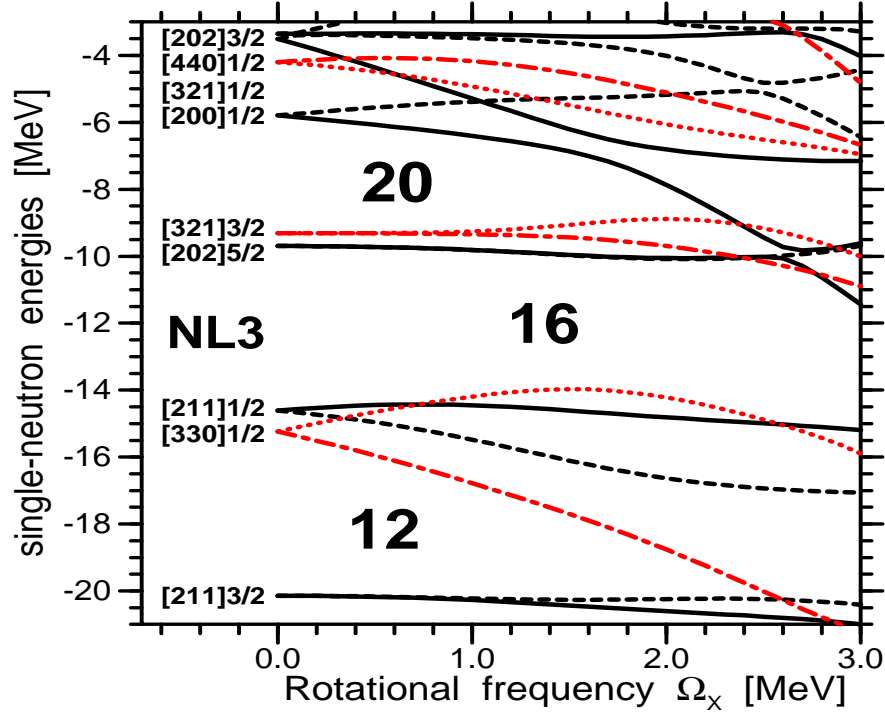


Figure 5: Neutron single-particle energies (routhians) obtained in the CRMF theory as a function of the rotational frequency Ω_x . They are given along the deformation path of the doubly-magic SD configuration [2,2] in ^{32}S . Solid, short-dashed, dot-dashed and dotted lines indicate $(\pi = +, r = -i)$, $(\pi = +, r = +i)$, $(\pi = -, r = +i)$ and $(\pi = -, r = -i)$ orbitals, respectively. At $\Omega_x = 0.0$ MeV, the single-particle orbitals are labeled by means of the asymptotic quantum numbers $[N n_z \Lambda] \Omega$ (Nilsson quantum numbers) of the dominant component of the wave function.

CRMF results for the $r_{tot} = -1$ configurations differ considerably from the ones obtained in the Skyrme calculations [22] where it was found that the $r_{tot} = -1$ configurations are not affected by the time-odd interactions (i.e. the interactions which give the time-odd mean fields through the Hartree-Fock averaging), while the $r_{tot} = +i$ configurations are significantly affected and acquire an additional binding.

When discussing the general structure of the high-spectra in the $A \sim 30$ mass region, one should remember that similar to the $A \sim 60$ mass region it is reasonable to expect that non-collective structures will compete with SD ones for yrast status in some spin range. Considering that self-consistent microscopic mean field theories have been applied so far only to the description of few cases of such coexistence (see section 8 in Ref. [4] for review) and that such description requires further development of relevant computer codes, we use here the configuration-dependent cranked Nilsson-Strutinsky (CNS) approach for outlining the general structure of high-spin spectra in the $A \sim 30$ mass region. The results of the CNS calculations are shown in Fig. 6.

In the case of ^{32}S , the SD configuration with the structure [2,2] is yrast from spin $I = 12\hbar$. It is interesting to mention that in the spin range $I = 6 - 10\hbar$, the yrast line is dominated by the aligned single-particle states in the CNS calculations. This feature has not been seen in previous microscopic self-consistent calculations which were restricted to collective shapes. Both the CRMF (Fig. 4) and CNS calculations show a large gap between the doubly magic yrast and the excited SD configurations.

In heavier nuclei, the observed SD bands are generally formed when the orbitals below the 2:1 harmonic oscillator gaps and, in addition, a few upsloping orbitals above these gaps are occupied.

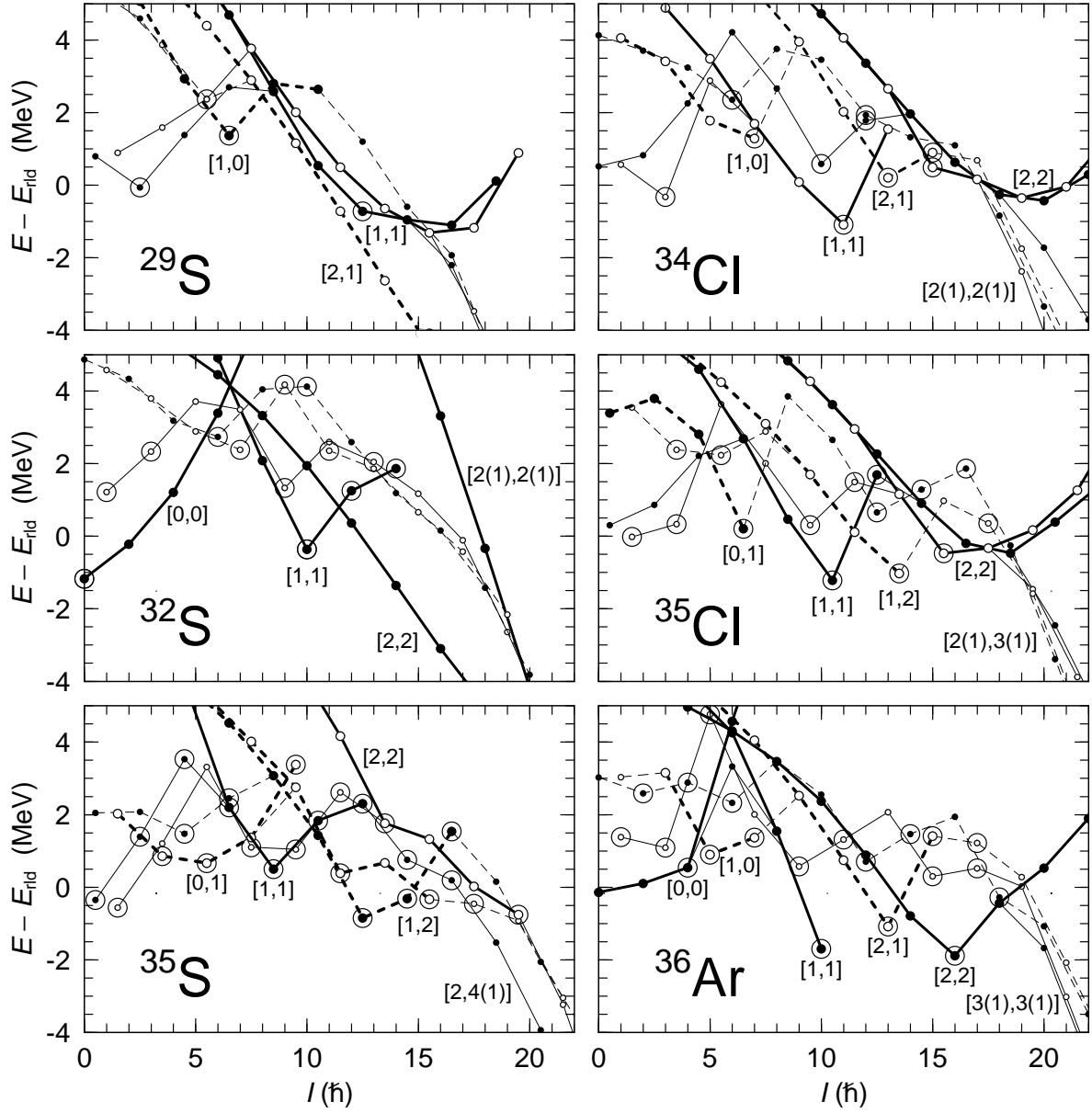


Figure 6: Low-lying configurations for selected nuclei in the $A = 29 - 36$ region calculated in the configuration dependent CNS approach. The energies are drawn relative to a standard rigid rotor reference [4]. Note that in Fig. 4 different reference is used in order to show the SD bands in more details. Full (dashed) lines are used for positive (negative) parity. Filled symbols indicate total signature $\alpha = 0$ ($r_{tot} = +1$) or $\alpha = 1/2$ ($r_{tot} = -i$) and open symbols are used for total signature $\alpha = 1$ ($r_{tot} = -1$) or $\alpha = -1/2$ ($r_{tot} = +i$). Aligned non-collective states are encircled. The yrast lines for the four combinations of signature and parity are drawn by thin lines while selected fixed configurations are shown by thicker lines. The strongly downsloping lines at the highest spin values correspond in general to configurations at deformations beyond $\varepsilon = 0.6$, typically with one or two particles excited to the $g_{9/2}$ subshell.

For example, in the $N = 86$ configuration of ^{152}Dy , the orbitals which are occupied in addition to those below the 2:1 $N = 80$ gap are $[642]5/2$, $[523]7/2$ and $[404]9/2$. Similarly, starting from the harmonic oscillator 2:1 gap for 16 particles, another favored configuration is formed if the $[202]5/2$ orbital above this gap is occupied by two protons and two neutrons. This configuration appears to be responsible for the recently observed SD band in ^{36}Ar [2]. In order to further analyze this configuration with 4 particles excited to the fp -shell, it appears interesting to investigate how it develops when starting from ^{32}S , the $[202]5/2$ nucleons are added one by one. Thus, the rotational bands for selected nuclei in this region, calculated in the CNS approach, are drawn in Fig. 6. Note that in these calculations, the proton and neutron single-particle orbitals are almost identical so the calculations for one nucleus can also be considered as a prediction for its mirror nucleus.

The configurations in these nuclei can be characterized by the number of protons and neutrons in the fp -shell which also determines the number of the holes in the sd -shell. It is evident from Fig. 6 that the yrast region is characterized by a number of aligned terminating states. These are formed as the maximum spin states within specific configurations. The orbital occupation in these aligned states is straightforward to identify, noting that one proton or neutron in the $N = 3$ shell will at most contribute with $7/2\hbar$ while two particles of the same kind in this shell contribute with $6\hbar$. These states are formed at a pretty large oblate deformation $\varepsilon_2 = 0.2 - 0.4$ which means that the two first holes in the $N = 2$ shell will be formed in the $[220]1/2$ orbital (which is upsloping with increasing oblate deformation) and therefore do not give any spin contribution in the fully aligned state. The next holes are formed in the $[211]3/2$ and $[211]1/2$ orbitals, thus giving a spin contribution of $3/2\hbar$ for the third hole, $2\hbar$ for four holes and $3/2\hbar$ for five holes. Higher spin states are formed if the last hole(s) are formed in the $[202]3/2$ and/or the $[202]5/2$ orbitals, but the states with holes in these orbitals are generally calculated to be less favored energetically (because of the large oblate deformation). These ‘rules’ suggest that favored aligned states should be formed at $I = 10\hbar$ in the $[1,1]$ configurations (with one $f_{7/2}$ proton and one $f_{7/2}$ neutron) both in ^{32}S (5+5 holes in the sd -shell) and in ^{36}Ar (3+3 holes) as confirmed by the full calculations, see Fig. 6. Comparing the three isotopes ^{29}S , ^{32}S and ^{35}S , one can notice a trend that when the number of neutrons comes closer to $N = 20$, the yrast line is more dominated by aligned states while more collective bands are formed for smaller neutron numbers.

The SD bands mentioned above are formed in the $[2,2]$ configurations. The calculations suggest that such a band is relatively low in energy in ^{32}S , somewhat higher in ^{36}Ar and even higher in the intermediate nuclei ^{35}Cl , ^{34}Cl and ^{33}S , the latter nucleus not shown in Fig. 6. The deformation at low spin in these bands varies continuously from $\varepsilon_2 \approx 0.4$ in ^{36}Ar to $\varepsilon_2 \approx 0.6$ in ^{32}S . The ^{36}Ar band approaches termination at $I = 16\hbar$ continuously, see Ref. [2], while the ^{32}S band is calculated only to decrease its deformation marginally reaching $\varepsilon_2 \approx 0.57$ ($\gamma \approx 4^\circ$) at $I = 18\hbar$ before the deformation starts to increase at even higher spin values. The kinematic and dynamic moments of inertia of this configuration are shown in Fig. 4b. In ^{34}Cl , four $[2,2]$ bands which are close to signature degenerate are formed, two of which are shown in Fig. 6. Their deformation decreases from $\varepsilon_2 \approx 0.5$ at low spin to $\varepsilon_2 \approx 0.4$ ($\gamma = 10 - 15^\circ$) at $I \approx 18\hbar$ and then increases at higher spin values. For one of the bands, see Fig. 6, this smooth trend is ‘interrupted’ by one aligned state at $I = 15\hbar$ formed according to the rules outlined above. The trends calculated for these bands are in general agreement with the harmonic oscillator rules presented in Ref. [29] (see also Ref. [4]) showing a division at a ground state deformation of $\varepsilon_2 \approx 0.5$ ($\gamma = 0^\circ$) between bands which terminate and bands which stay collective for all spin values, reaching very large

deformations in the limit of very high spin values.

4 Conclusions

The rotational properties of SD bands in the ^{59}Cu - ^{60}Zn - ^{61}Zn nuclei, which are expected to be influenced by the proton-neutron pairing correlations, have been compared with the ones of SD bands around ^{150}Gd , where the proton-neutron pairing plays no role. The similarity of the experimental situation in these two regions suggests that the presence of a jump in the dynamic moment of inertia $J^{(2)}$ of the SD band in ^{60}Zn and the absence of such jumps in the neighboring nuclei ^{59}Cu and ^{61}Zn cannot be considered as a clear signal of proton-neutron pairing correlations. It rather suggests a strong dependence of the 'expected' proton and neutron band crossings properties on the deformation of the system. Deformation effects should be more pronounced in the $A \sim 60$ mass region where the relative polarization effects induced by the additional particle(s) are larger than in the $A \sim 150$ region. For example, the main features of a paired band crossing in the SD band of ^{60}Zn can be understood in the cranked relativistic Hartree-Bogoliubov theory without an explicit proton-neutron pairing. This does not imply, however, that there is no proton-neutron pairing but suggests that it does not play a dominant role in the definition of the properties of paired band crossings at superdeformation in the $A \sim 60$ mass region.

A number of issues such as the high-spin structure of ^{32}S at superdeformation, rotational properties at superdeformation, the role of nuclear magnetism (time-odd components of the mean field) in the signature splitting of excited SD bands has been investigated within the cranked relativistic mean field theory. In addition, the general structure of high-spin spectra in the $A \sim 30 - 35$ mass region has been studied in the configuration-dependent CNS approach with main emphasis on the coexistence of collective and non-collective structures along the yrast line and the particle number dependence of the SD configurations with two protons and two neutrons in the fp -shell.

Acknowledgements:

A.V.A. acknowledges support from the Alexander von Humboldt Foundation. This work is also supported in part by the Bundesministerium für Bildung und Forschung under the project 06 TM 979 and by the Swedish Natural Science Research Council.

References

- [1] C. E. Svensson *et al.*, Phys. Rev. Lett. **79**, 1233 (1997).
- [2] C. E. Svensson *et al.*, subm. to Phys. Rev. Lett. and these proceedings.
- [3] A. V. Afanasjev, I. Ragnarsson and P. Ring, Phys. Rev. C **59**, 3166 (1999).
- [4] A. V. Afanasjev, D. B. Fossan, G. J. Lane and I. Ragnarsson, Phys. Rep. **322**, 1 (1999).
- [5] C.-H. Yu *et al.*, Phys. Rev. C **60**, 031305 (1999).
- [6] C. Andreoiu *et al.*, submitted to Phys. Rev. C. and these proceedings.
- [7] W. Koepf and P. Ring, Nucl. Phys. A **493**, 61 (1989).
- [8] A. V. Afanasjev, J. König and P. Ring, Nucl. Phys. A **608**, 107 (1996).
- [9] A. V. Afanasjev, P. Ring and J. König, Nucl. Phys. A, in press (see also report nucl-th/0001054).
- [10] C. E. Svensson *et al.*, Phys. Rev. Lett. **80**, 2558 (1998).
- [11] A. Galindo-Uribarri *et al.*, Phys. Lett. B **422**, 45 (1998).
- [12] C. E. Svensson *et al.*, Phys. Rev. Lett. **82**, 3400 (1999).

- [13] M. Devlin *et al.*, Phys. Rev. Lett. **82**, 5217 (1999).
- [14] A. V. Afanasjev, G. A. Lalazissis and P. Ring, Nucl. Phys. **A 634**, 395 (1998).
- [15] S. G. Frauendorf and J. A. Sheikh, Nucl. Phys. **A 645**, 509 (1999).
- [16] S. Frauendorf and J. A. Sheikh, Phys. Rev. **C 59**, 1400 (1999).
- [17] W. Nazarewicz, R. Wyss and A. Johnson, Nucl. Phys. **A 503**, 285 (1989).
- [18] A. V. Afanasjev, J. König and P. Ring, Phys. Rev. **C 60**, 051303 (1999).
- [19] Y. Sun, J. Zhang, M. Guidry and C.-L. Wu, Phys. Rev. Lett. **83**, 686 (1999).
- [20] R. K. Sheline, I. Ragnarsson and S. G. Nilsson, Phys. Lett. **41B**, 115 (1972).
- [21] G. Leander and S. E. Larsson, Nucl. Phys. **A 239**, 93 (1975).
- [22] H. Molique, J. Dobaczewski and J. Dudek, Phys. Rev. **C 61**, 044304 (2000) and these proceedings.
- [23] M. Yamagami and K. Matsuyanagi, Nucl. Phys. **A 672**, 123 (2000) and these proceedings.
- [24] T. Tanaka, R. G. Nazmitdinov and K. Iwasawa, report nucl-theor/0004009 (2000).
- [25] R. R. Rodriguez-Guzmán, J. L. Egido and L. M. Robledo, report nucl-th/0006013 (2000).
- [26] G. A. Lalazissis, J. König and P. Ring, Phys. Rev. **C 55**, 540 (1997).
- [27] I. Ragnarsson, Phys. Lett. **B 199**, 317 (1987).
- [28] A. V. Afanasjev and P. Ring, in preparation.
- [29] T. Troudet and R. Arvieu, Z. Phys. **A 291**, 183 (1979); Annals of Physics **134**, 1 (1981).